

Synthesis and Characterization of Novel Heat Resistant, Superparamagnetic Poly(ether-imide) Nanocomposites Containing Xanthene: Representing a Strategy for Improving Thermal Stability of Magnetic Polymer-Based Nanocomposites

Akbar Mobinikhaledi¹ · Hassan Moghanian² · Parvin Safari¹ · Elnaz Firuzian¹

Received: 2 September 2017 / Accepted: 20 October 2017 / Published online: 27 October 2017
© Springer Science+Business Media, LLC 2017

Abstract Two superparamagnetic and heat resistant xanthene based poly(ether-imide) nanocomposites were successfully synthesized. Field emission scanning electron microscopy, transmission electron microscope, X-ray diffraction, thermal gravimetric analysis, vibrating sample magnetometer, Energy-dispersive X-ray spectroscopy and Fourier-transform infrared (FTIR) techniques were used for studying the morphology, crystalline phase, thermal stability and magnetization properties of the nanocomposites. The neat form of the corresponding poly(ether-imide) was also prepared by thermal imidization method and its structure was confirmed by FTIR, proton nuclear magnetic resonance (¹H NMR), UV–Vis and photoluminescence (PL) spectroscopies. In order to investigate the effects of modifying the surface of Fe₃O₄ nanoparticles on thermal properties of the nanocomposites, the surface of Fe₃O₄ nanoparticles was coated with SiO₂ and polysuccinimide (PSI), sequentially. Then, both the unmodified Fe₃O₄ and surface-modified Fe₃O₄ (Fe₃O₄@SiO₂-PSI) nanoparticles were used as fillers for the polymer matrix. According to the results, the prepared nanocomposites were superparamagnetic and showed higher thermal stability in comparison to the neat poly(ether-imide). Furthermore, poly(ether-imide)/Fe₃O₄@SiO₂-PSI (PIEN 10b) nanocomposite showed higher thermal stability and dispersed better in the polymer matrix [in comparison to poly(ether-imide)/Fe₃O₄ (PIEN 10 a)] due to the presence of imide groups and high hydroxyl content of the functional

Fe₃O₄ nanoparticles which caused high interactions between poly(ether-imide) and functional Fe₃O₄. Furthermore, the presence of methyl, ether and bulky xanthene groups in the poly(ether-imide)(backbone improved the solubility of the neat polymer in organic solvents. These properties can be very helpful for extending new applications of poly(ether-imide)s.

Keywords Heat resistant nanocomposites · Xanthene · Poly(ether-imide) · Superparamagnetism · Fe₃O₄ nanoparticles

1 Introduction

Inorganic nanomaterials incorporation into the polymer matrix (polymer nanocomposites) have attracted both academic and industrial attentions during the last few decades due to their improved chemical resistance, thermal stability, electrical conductivity, mechanical properties, flame retardancy [1], easy process ability and low-cost manufacturing [2]. Especially, magnetic polymer materials can show many potential applications in electromagnetic interference shielding, electronic devices, cell separation, magnetic recording materials, drug targeting, magnetic sensors and energy storage devices [3].

Also, among the inorganic nanomaterials, magnetite (Fe₃O₄) is a great candidate for the synthesis of polymer nanocomposites due to its promising electromagnetic properties, superparamagnetic [4], biocompatibility [5], ease of synthesis [6], nontoxicity [7], high specific surface area, high coercivity and chemical catalytic properties [8, 9]. Especially, the presence of superparamagnetism property in nanocomposites makes Fe₃O₄ interesting for medical purposes, such as drug delivery and therapy [10, 11]. However, researchers

✉ Akbar Mobinikhaledi
akbar_mobini@yahoo.com

¹ Department of Chemistry, Faculty of Science, Arak University, Arak 38156-8-8349, Iran

² Department of Chemistry, Dezful Branch, Islamic Azad University, Dezful, Iran

have to face some major challenges in preparing well dispersed Fe_3O_4 /polymer nanocomposites because of the agglomeration tendency of Fe_3O_4 nanoparticles which is derived from their high specific surface areas and strong magnetic dipole–dipole interactions between these nanoparticles [12]. The surface modification of Fe_3O_4 nanoparticles can prevent from the self-aggregation of nanocomposites [13, 14] and also it can improve their chemical stability, dispersion in various matrixes and stability in low pH values [15].

Polyimides (PI) are very useful for advanced technologies because of their excellent thermal stability, superior chemical resistance and improved mechanical properties [16]. These polymers have various applications in micro-electronics, composites, automobile, aerospace, coatings, and membranes [17, 18]. Also, they are interesting matrixes for the preparation of nanocomposite materials because of their unique properties [19–23]. Therefore, academic and industrial researchers have extensively focused on developing optimum methods for producing new polyimide materials to further enhance their desirable properties and applications [24]. However, these polymers are very rigid and their applications have been limited by their poor thermoplastic fluidity and solubility. Using poly(ether-imide)s instead of polyimides can prevent from the limitations mentioned above. Poly(ether-imide)s can provide good processability and solubility due to the presence of flexible ether links in their structures. Furthermore, incorporating large heterocycles; like xanthenes, into the main chain of the poly(ether-imide)s can further improve the good properties of these polymers [25].

The aim of this work was to represent a method for improving good properties of polymer based magnetic nanoparticles. In order to fulfill this objective, the surface of Fe_3O_4 were coated with SiO_2 and polysuccinimide and the modified Fe_3O_4 were utilized for the synthesis of a new xanthene based poly(ether-imide) nanocomposite (poly(ether-imide)/ Fe_3O_4 @ SiO_2 -PSI). The neat form of this polymer and the corresponding polymer nanocomposite derived from unmodified Fe_3O_4 (poly(ether-imide)/ Fe_3O_4) were also prepared to compare with poly(ether-imide)/ Fe_3O_4 @ SiO_2 -PSI. The prepared nanocomposites were superparamagnetic and had higher thermal stability than the neat polymer. Also, poly(ether-imide)/ Fe_3O_4 @ SiO_2 -PSI was thermally more stable than poly(ether-imide)/ Fe_3O_4 because surface modification improved the interaction of the magnetic nanoparticles with the polymer matrix.

2 Experimental

2.1 Materials and Methods

All reagents were bought from Merck, Sigma-Aldrich and Fluka companies and used without further purification.

The melting points were determined by Electrothermal 9200 apparatus and a Galaxy series FTIR 5000 spectrometer was used for recording FTIR spectra, in the range of 400–4000 cm^{-1} . The ^1H and ^{13}C NMR spectra were recorded on a Bruker Avance spectrometer operating at 400 and 100 MHz for ^1H and ^{13}C , respectively. Also, a TGA/DTA instrument (a Mettler TA4000 System) was applied for the characterization of the nanocomposites. The X-ray diffraction (XRD) was performed on Philips X-Pert (Cu-K α radiation, $\lambda=0.15405$ nm) in the range of $2\theta=20^\circ$ – 80° with 0.04° as the step length. A Hitachi S-4700 field emission-scanning electron microscope (FE-SEM) and a transmission electron microscopy (TEM with microscope LEO) were utilized for the study of particle size and external morphology. The magnetization of the nanoparticles was detected by using a Vibrating Sample Magnetometer (Model 7300 VSM system, Lake Shore Cryotronic, Inc., Westerville, OH, USA) at room temperature. Finally, UV–Vis spectra were recorded by using a Perkin Elmer Lambda 15 spectrophotometer in N,N-dimethylformamide (DMF) at 25 °C in the range of 190–790 nm.

2.2 Monomer Synthesis

The procedures reported in the literature [26] were used for the synthesis of 4,4'-(((4-(14H-dibenzo[a,j]xanthen-14-yl)phenyl)methylene) bis(2,5-dimethyl-4,1-phenylene)) bis(oxy)) dianiline (BXOA). This synthesis route consisted of four steps and the spectral data of all of the products were in good agreement with the reported results in the literature.

2.2.1 Preparation of 4-(14H-dibenzo[a,j]xanthen-14-yl) benzaldehyde (BXB)

Terephthalaldehyde (20 mmol), 2-naphthol (45 mmol) and p-TSA (1 mmol) were added to 1,2-dichloroethane (120 mL) and the solution was refluxed under nitrogen atmosphere for 24 h. Next, the organic solvent was evaporated and a mixture of ethanol:water (3:1) was added to the residue. Finally, the precipitate was filtered and washed with ethanol several times. Yield = 90%; Melting point (Mp): 328–333 °C.

2.2.2 Preparation of 4,4'-((4-(14H-dibenzo[a,j]xanthen-14-yl)phenyl)methylene) bis(2,5-dimethylphenol) (BXOH)

2,5-Dimethylphenol (35 mmol), BXB (15 mmol) and pTSA (1 mmol) were mixed and heated to 120 °C for 1 h under solvent-free conditions. At this time, the mixture was cooled to room temperature and a mixture of ethanol:water (2:1) was added to it. After stirring for 10 min at room temperature, the product was filtered and dried. Yield = 92%; M.p: 310–312 °C.

2.2.3 Synthesis

of 14-(4-(bis(2,5-dimethyl-4-(4-nitrophenoxy)phenyl)methyl)phenyl)-14H-dibenzo[a,j] xanthene (BXNO₂)

The solid obtained in the previous step (BXOH, 12 mmol), 4-fluoro nitrobenzene (30 mmol) and potassium carbonate (24 mmol) were dissolved in DMF (50 mL) and then the solution was refluxed for 24 h. After cooling, cold water (200 mL) was added to the solution. The obtained yellow crude product was filtered and washed with hot ethanol. Yield=85%; M.p=311–314 °C.

2.2.4 Synthesis of 4,4'-(((4-(14H-dibenzo[a,j]

xanthen-14-yl)phenyl)methylene)bis(2,5-dimethyl-4,1-phenylene))bis(oxy)dianiline (BXOA)

A mixture of BXNO₂ (5 mmol) and palladium on carbon (Pd/C) 10% (0.5 g) was added to the mixture of ethanol:THF (120 mL, 5:1) and the mixture was heated to 70 °C. Then, a solution of hydrazine monohydrate 80% (8 mL in 15 mL of ethanol) was added dropwise by using a dropping funnel during 30 min and the mixture was refluxed for 2 h. Next, the hot mixture was filtered in order to remove Pd/C. Finally, the solvent was evaporated under vacuum and the white product was washed thoroughly with ethanol and dried. In continue, the spectral data of this compound have been reported. Yield=94%; M.p=182–183 °C.

FTIR (KBr): ν_{\max} = 3449, 3380, 3042, 2920, 1620, 1501, 1398, 1246, 1208, 1068, 902, 820, 720, 507 cm⁻¹. ¹H NMR (400 MHz, DMSO-d₆): 8.65 (d, *J*=8.4 Hz, 2H), 7.93 (d, *J*=9.2 Hz, 4H), 7.63 (t, *J*=14.4 Hz, 2H), 7.55 (t, *J*=16.4 Hz, 4H), 7.46 (t, *J*=15.2 Hz, 2H), 6.83 (d, *J*=8 Hz, 2H), 6.70 (s, 1H), 6.62 (d, *J*=8.4 Hz, 4H), 6.52 (d, *J*=8.4, 4H), 6.38 (s, 2H), 6.23 (s, 2H), 5.30 (s, 1H), 4.87 (br, 4H), 1.88 (s, 6H), 1.82 (s, 6H) ppm. ¹³C NMR (100 MHz, DMSO-d₆): δ = 154.3, 147.9, 146.4, 144.7, 144.6, 143.3, 140.5, 135.3, 134.4, 130.9, 130.6, 129.2, 129, 128.6, 128.0, 126.8, 124.4, 123.6, 123.3, 119.7, 117.9, 117.6, 117.2, 114.8, 47.6, 36.3, 18.9, 15.7 ppm.

2.3 Synthesis of the New Xanthene Based Poly(ether-imide) (XBPEI)

The new poly(ether-imide) was synthesized by thermal imidization method. BXOA (0.4 mmol) was dissolved in N,N-dimethylacetamide (DMAc) (5 mL). While the solution was stirring at room temperature, 4,4'-oxydiphthalic anhydride (0.124 g) was slowly added to it. The solution was stirred at room temperature under nitrogen atmosphere overnight to synthesize poly(amic acid) (PAA). Next, the PAA solution was poured into a glass dish and heated with a programmed

temperature at 80, 110, 140, 170 and 200 °C for 10 h in a vacuum oven.

2.4 Preparation of the Magnetic Nanoparticles

2.4.1 Synthesis of Fe₃O₄ Magnetic Nanoparticles

Fe₃O₄ nanoparticles were synthesized by chemical co-precipitation method [27]. A mixture of FeCl₂·4H₂O (5 mmol) and FeCl₃·6H₂O (10 mmol) was added to deionized water (100 mL) in a three-necked round bottomed flask. The solution was heated for 1 h at 80 °C under N₂ atmosphere. Then, concentrated ammonia (10 mL, 25%) was quickly added to the solution and the resulting solution was stirred for another 1 h. Next, the mixture was cooled to room temperature and the prepared magnetic nanoparticles were isolated by using an external magnet, washed with deionized water and ethanol, and finally dried under vacuum at room temperature.

2.4.2 Synthesis of Silica-Coated Fe₃O₄ (Fe₃O₄@SiO₂)

Stober method was utilized for the synthesis of Fe₃O₄@SiO₂ core-shell nanoparticles [28]. Fe₃O₄ nanoparticles (0.5 g) were sonicated in a mixture of ethanol (40 mL), deionized water (6 mL) and concentrated aqueous ammonia solution (1.5 mL, 25 wt%) for 30 min. Subsequently, 1.4 mL of tetraethyl orthosilicate (TEOS) was added dropwise and the mixture was stirred for 12 h at room temperature under N₂ atmosphere. Finally, the product was separated from the solution by using a magnet, washed with deionized water and ethanol several times and dried under vacuum at 25 °C.

2.4.3 Synthesis of 3-Aminopropyl-Functionalized Magnetic Silica Nanoparticles (Fe₃O₄@SiO₂-NH₂)

Fe₃O₄@SiO₂ (0.5 g) and (3-aminopropyl) triethoxysilane (APTES, 3 mL) were added to toluene (50 mL) and the mixture was completely dispersed by using ultrasonic vibrations. Consequently, the mixture was refluxed with continuous stirring for 24 h under nitrogen atmosphere. Next, the product was collected by using an external magnet, washed with toluene and ethanol several times and dried at 60 °C for 6 h.

2.4.4 Preparation of Fe₃O₄@SiO₂-PSI

Scheme 1 illustrates the synthesis route for Fe₃O₄@SiO₂-PSI nanoparticles. A mixture of Fe₃O₄@SiO₂-NH₂ (0.5 g), aspartic acid (1.5 g) and phosphoric acid (2 g) was poured into a large test tube and heated to 200 °C for 6 h under nitrogen atmosphere. Then, the residue was washed with hot dimethyl sulfoxide (DMSO) several times and dried at 60 °C in a vacuum oven.

2.5 Preparation of Poly(ether-imide)/Fe₃O₄ (PIEN 10a) and Poly(ether-imide)/Fe₃O₄@SiO₂-PSI (PIEN 10b) Nanocomposites

BXOA (0.4 mmol) was dissolved in DMAc (5 mL) and 4,4'-oxydiphthalic anhydride (0.4 mmol) was slowly added to it. The solution was vigorously stirred at room temperature for 24 h under N₂ atmosphere to form PAA. The suspension of Fe₃O₄ or Fe₃O₄@SiO₂-PSI (0.017 g) in DMAc (1 mL) was prepared by sonicating for 1 h and then added to the PAA solution. The mixture was stirred at room temperature overnight under nitrogen atmosphere. The resulting mixture was poured into a glass petri dish and step heating were carried out at the temperatures of 80, 110, 140, 170 and 200 °C, respectively (each step for 2 h) to form the nanocomposites.

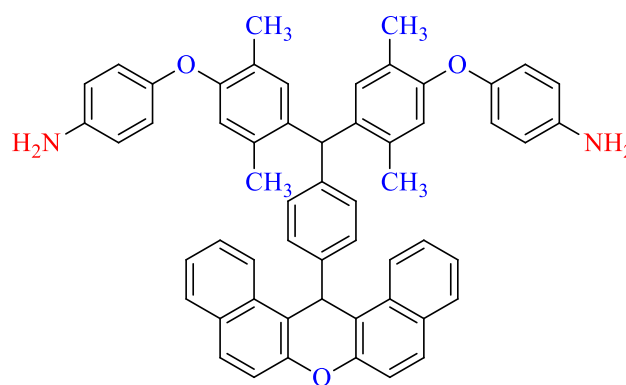
3 Results and Discussions

3.1 Characterization of 4,4'-((((4-(14H-dibenzo[a,j]xanthen-14-yl)phenyl)methylene)bis(2,5-dimethyl-4,1-phenylene))bis(oxy))dianiline (BXOA)

Scheme 2 illustrates the proposed structure for BXOA monomer. This compound was characterized by FTIR, ¹H NMR and ¹³C NMR

In the FTIR spectrum of BXOA, the bands appeared at 3380 and 3449 cm⁻¹ were assigned to symmetric and asymmetric stretching vibrations of NH₂ groups, respectively. Also, an absorption band was observed at 3042 cm⁻¹ which corresponded to the aromatic C–H stretching vibrations. The band related to C–O stretching vibrations appeared as a very sharp band at 1246 cm⁻¹.

According to the ¹H NMR spectrum of BXOA, the singlet signals at 1.82 and 1.88 ppm (each 6H) were ascribed to the methyl groups and the resonance of NH₂ protons caused the appearance of the singlet signal at 4.87 ppm (4H). The signals centered at 5.30 and 6.70 ppm (each 1H) were assigned



Scheme 2 The proposed structure for the monomer (BXOA)

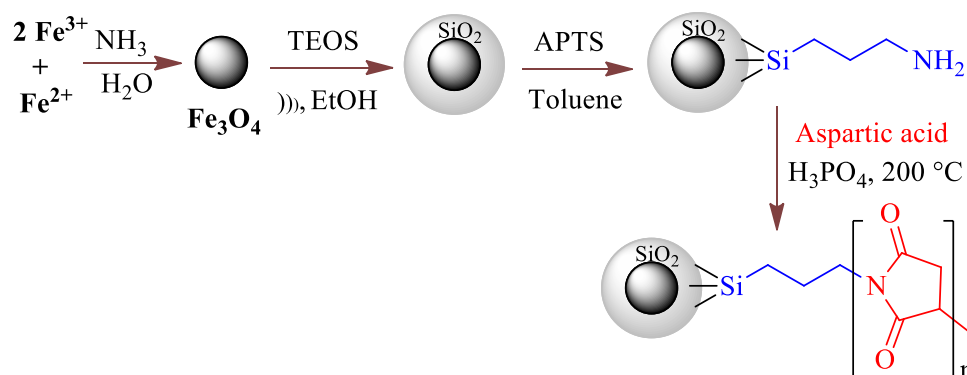
to the protons of aliphatic C–H center (in the ortho position of methyl groups) and aliphatic C–H in xanthene ring, respectively. Finally, the signals derived from the resonance of the aromatic protons appeared between 6.23 and 8.65 ppm (totally 28H).

The additional confirmation for the proposed structure of BXOA was obtained from ¹³C NMR spectrum. Four signals appeared in the region of 15.7–47.6 ppm were assigned to aliphatic carbons and twenty-four signals observed between 114.8 and 154.3 ppm were related to the resonance of aromatic carbons.

3.2 Characterization of the Xanthene Based New Poly(ether-imide) (XBPEI)

The presence of flexible aliphatic side chains with different functionalities in the structure of aromatic polyimides can improve the processability and decrease Tg without any loss in their important properties. Furthermore, xanthene skeleton because of their steric bulk improve the solubility of the polymers. For this reason, we incorporated previously synthesized diamine [26] containing xanthene ring, ether groups and high content of methyl groups into the structure of our newly synthesized poly(ether-imide).

Scheme 1 Synthesis route for Fe₃O₄@SiO₂-PSI nanoparticles



A conventional two-step procedure was used for the synthesis of XBPEI (Scheme 3). The reaction between equal moles of the monomer (BXOA) and commercially available 4,4'-oxydipthalic anhydride (ODPA) in DMAc produced polyamic acid and then, this reaction followed by thermal cyclodehydration to give the new poly(ether-imide).

The chemical structure proposed for the newly synthesized polymer (XBPEI) was supported by the FTIR, ^1H NMR and elemental analysis techniques.

Figure 1 exhibits the FTIR spectrum of XBPEI. The bands assigned to the asymmetric and symmetric vibrations of N–H groups disappeared upon polymerization. This fact proved the successful formation of XBPEI. Also, the other bands appeared in the FTIR spectrum of XBPEI were completely consistent with the proposed structure. The bending vibrations of C=O groups caused an absorption band at 822 cm^{-1} . The band observed at 1236 cm^{-1} was arisen from C–O stretching vibrations of the xanthene ring and ether groups. The peak appeared at 1373 cm^{-1} was due to C–N stretching vibrations in the imide groups. The characteristic absorption band related to the symmetric and asymmetric carbonyl stretching vibrations of the imide groups appeared at 1724 and 1780 cm^{-1} , respectively. The peaks at 2865 and 2922 cm^{-1} were attributed to the symmetric and asymmetric vibrations of aliphatic C–H groups, respectively. Finally, the

absorption band at 3057 cm^{-1} was assigned to the stretching vibrations of aromatic C–H groups.

The successful polymer formation was also confirmed by ^1H NMR spectrum of XBPEI. The assignment for each proton has clearly been shown in Fig. 2. The peak at 4.87 ppm, which was related to the protons of amine groups, was disappeared after polymerization. This fact suggested that polymerization was performed efficiently. The singlet signals observed at 1.85 and 1.94 ppm were due to the proton resonance of methyl groups. Also, the resonance of the aliphatic proton of C–H center (j) appeared at 5.45 and the signals related to the aromatic protons and the aliphatic proton of xanthene appeared in the range of 6.40–8.81 ppm. Also, there was a good agreement between the elemental analysis values of this polymer and its calculated values.

3.3 Polymer Solubility

The solubility of this polymer was investigated by adding the polymer (0.01 g) to different solvents (2 mL). The synthesized polymer was easily soluble in polar aprotic solvents like DMF, DMAc, DMSO, tetrahydrofuran (THF) and N-methyl-2-pyrrolidone (NMP) at room temperature and insoluble in polar protic solvents like methanol, ethanol and water. This polymer showed an enhanced solubility in comparison to conventional aromatic polyimides. The

Scheme 3 Synthesis of the new poly(ether-imide) (XBPEI)

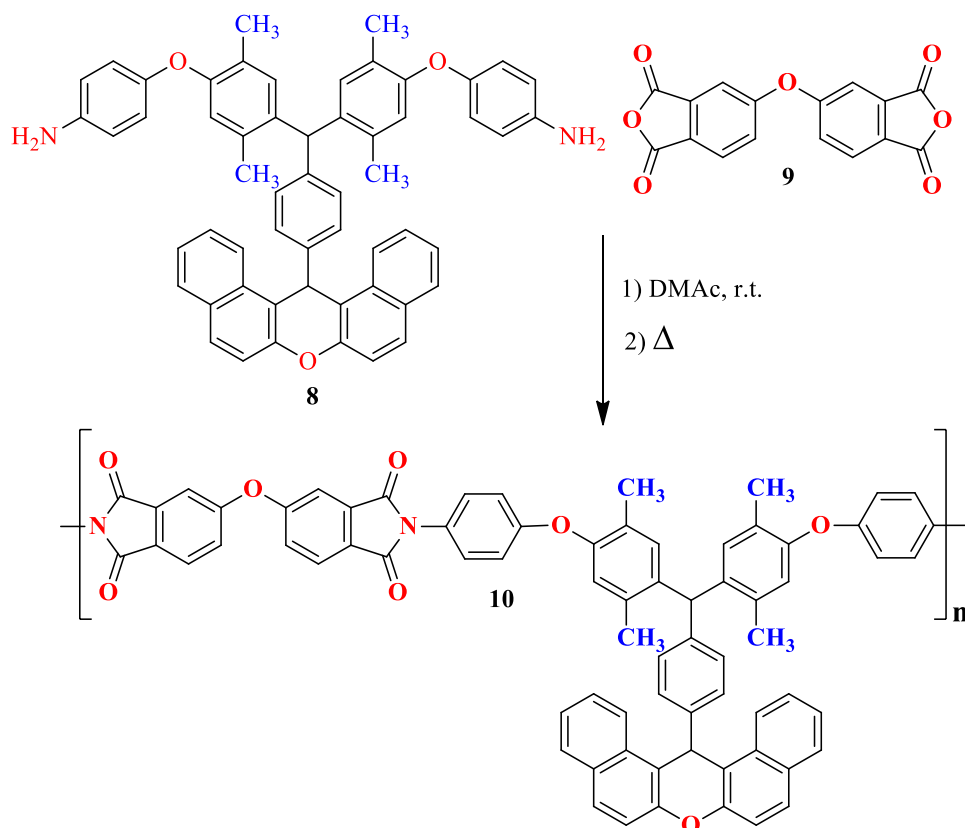


Fig. 1 FTIR spectrum of the new poly(ether-imide) (XBPEI)

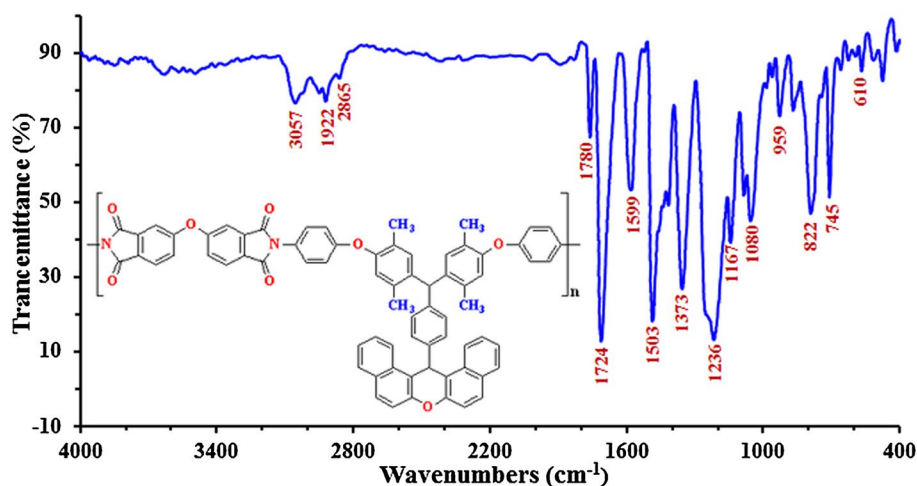
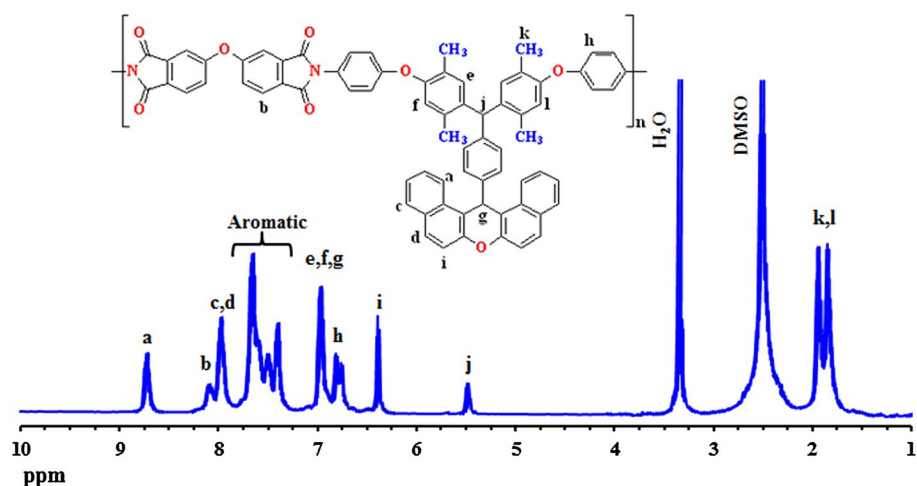


Fig. 2 ^1H NMR spectrum of the new poly(ether-imide) (XBPEI)



introduction of xanthene moiety, ether and aliphatic groups in the side chain of the polymer was the main reason for the good solubility of this polymer. In other word, the mentioned groups disturbed the dense packing of the polymer chains and increased the distances between the side chains. As a result, interactions between the chains decreased and consequently, the solvent molecules were able to penetrate into the polymer chains more easily.

3.4 Characterization of the Magnetic Nanocomposites

3.4.1 FTIR Spectroscopy

The FTIR spectra of Fe_3O_4 , $\text{Fe}_3\text{O}_4@\text{SiO}_2$ and $\text{Fe}_3\text{O}_4@\text{SiO}_2\text{-PSI}$ (in the range of 400–4000 cm^{-1}) have been shown in Fig. 3.

The characteristic bands observed at 576 cm^{-1} were assigned to Fe–O stretching vibrations. The absorption bands related to SiO_2 shells were detected by comparing the FTIR spectra of $\text{Fe}_3\text{O}_4@\text{SiO}_2$ and $\text{Fe}_3\text{O}_4@\text{SiO}_2\text{-PSI}$

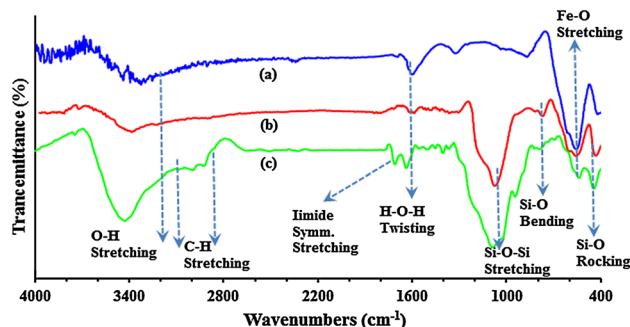


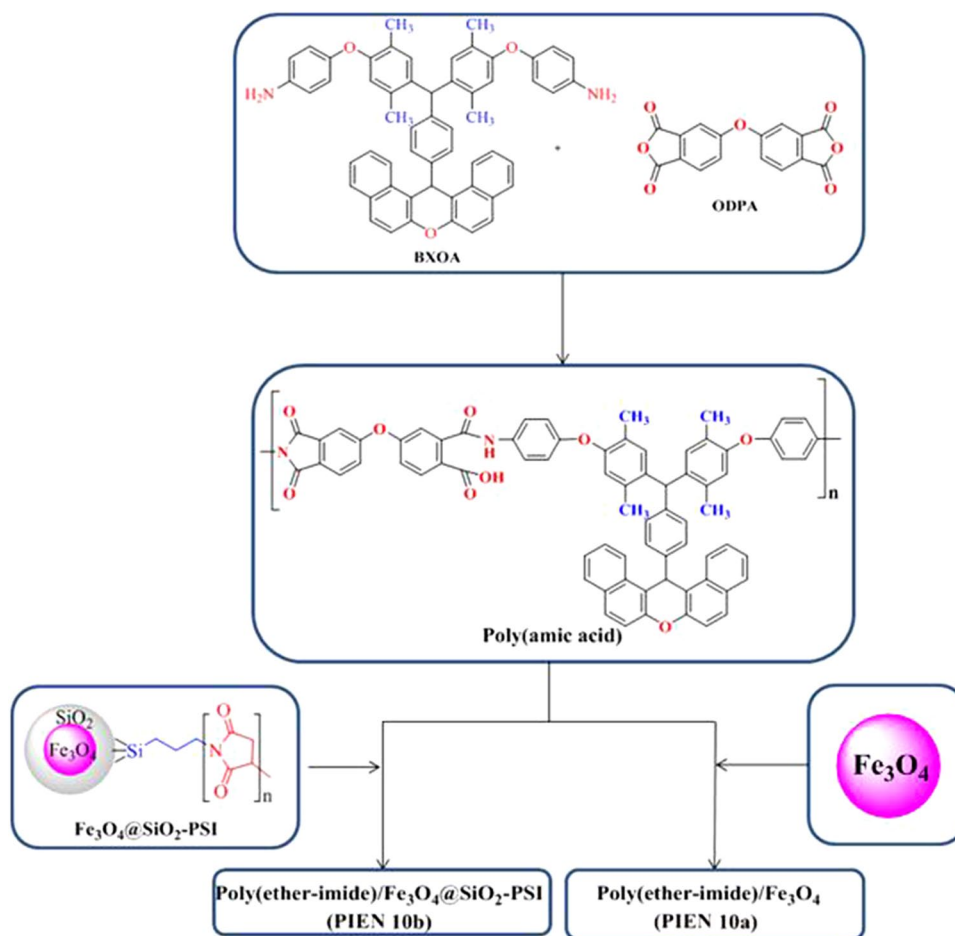
Fig. 3 FTIR spectra of Fe_3O_4 (a), $\text{Fe}_3\text{O}_4@\text{SiO}_2$ (b) and $\text{Fe}_3\text{O}_4@\text{SiO}_2\text{-PSI}$ (c)

with that of Fe_3O_4 . In the FTIR spectra of $\text{Fe}_3\text{O}_4@\text{SiO}_2$ and $\text{Fe}_3\text{O}_4@\text{SiO}_2\text{-PSI}$, there were sharp adsorption bands at 1090 cm^{-1} ; which were due to Si–O–Si asymmetric stretching vibrations; and three weak peaks at 950, 800 and 460 cm^{-1} ; which were ascribed to the symmetric stretching vibrations, in plane bending and rocking mode of Si–O–Si

groups; respectively. In the FTIR spectra of all three compounds, the bands appeared at 3400 and 1620 cm^{-1} were created by O–H stretching vibrations and H–O–H twisting vibration modes, respectively. The peaks appeared at 2963 and 2926 cm^{-1} , in the FTIR spectrum of Fe_3O_4 @ SiO_2 -PSI, were related to C–H asymmetric and symmetric stretching vibrations, respectively. Moreover, the FTIR spectrum of Fe_3O_4 @ SiO_2 -PSI illustrated three absorption bands at 1720, 1355 and 840 cm^{-1} due to C=O stretching vibration, C–N stretching vibration and C=O bending vibration in the imide moiety, respectively. These FTIR spectra proved that Fe_3O_4 , Fe_3O_4 @ SiO_2 and Fe_3O_4 @ SiO_2 -PSI were successfully synthesized.

Poly(ether-imide)/ Fe_3O_4 and poly(ether-imide)/ Fe_3O_4 @ SiO_2 -PSI nanocomposites were prepared by thermal imidization method. Figure 4 depicts the flowchart of the whole process for preparing these nanocomposite films.

Fig. 4 The flowchart of the whole process for preparing the nanocomposite films



3.5 Morphology Studies by Field Emission Scanning Electron Microscopy (FE-SEM) and Transmission Electron Microscopy (TEM)

FE-SEM was used to investigate the morphology of the nanocomposites and the extent of the dispersion of the fillers (Fe_3O_4 and Fe_3O_4 @ SiO_2 -PSI nanoparticles) in the polymer matrix. As can clearly be seen in Fig. 5, the presence of some functional groups, like imide, xanthene, and ether, in the structure of the polymer caused a very well dispersion of the fillers in the polymer matrix. However, the dispersion of Fe_3O_4 @ SiO_2 -PSI nanoparticles (Fig. 5b) were more homogeneous than that of Fe_3O_4 (Fig. 5a), indicating that hydroxyl and polysuccinimide groups (in the structure of the filler) had an important effect in the quality of the filler dispersion. Furthermore, Fe_3O_4 nanoparticles (Fig. 5b) showed a little aggregation which could be attributed to the strong van der Waals interactions between the nanoparticles [2].

In addition, Fig. 6 shows the typical morphology of PIEN 10b observed by TEM. Dark spots represent the magnetic nanoparticles while the background indicates the polymer matrix. It is clear from Fig. 6 that these nanoparticles were almost spherical and uniform in shape and their mean

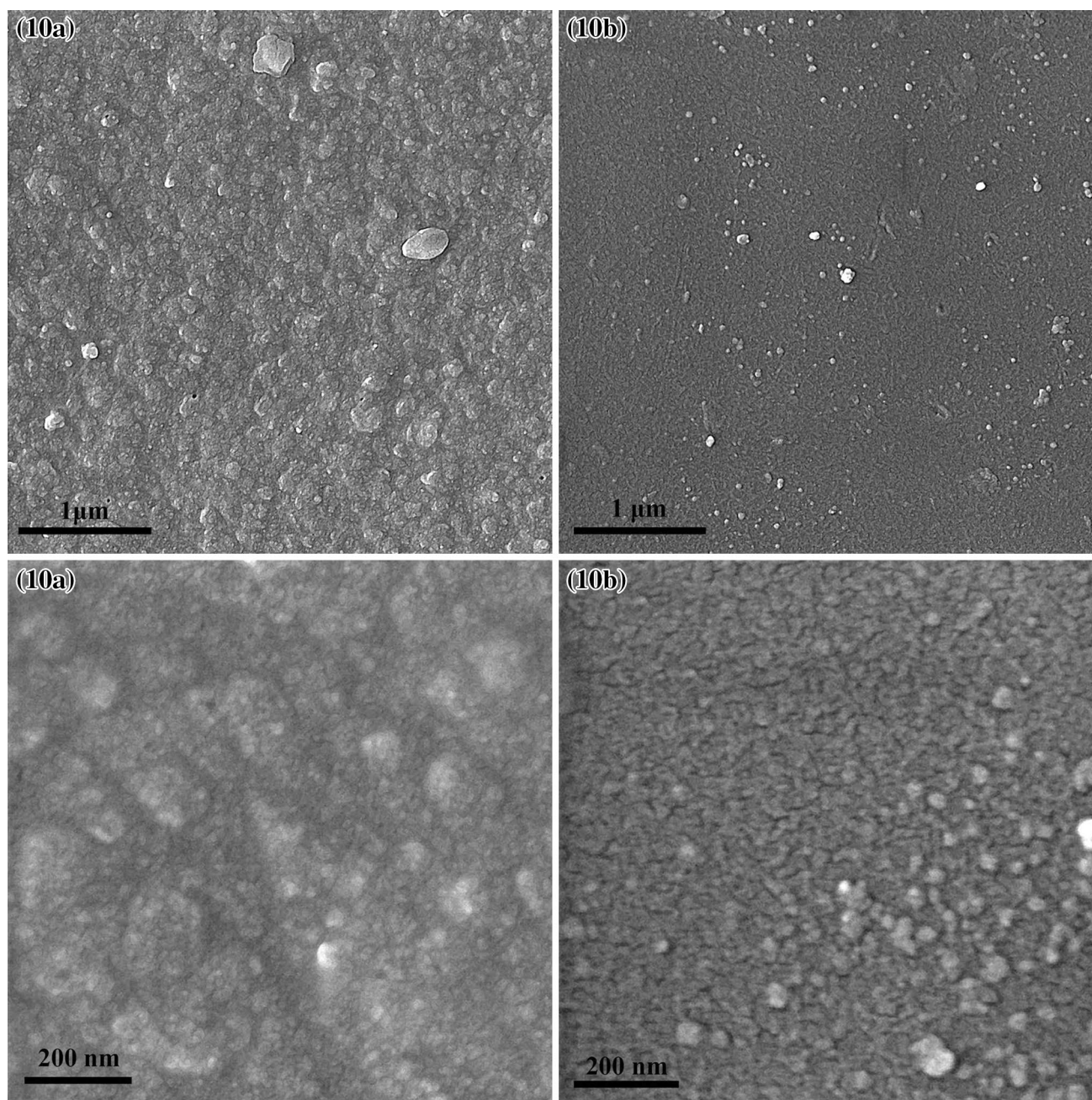


Fig. 5 FE-SEM images of **a** PIEN 10a and **b** PIEN 10b

diameter was about 6–18 nm. According to TEM analysis, the magnetic $\text{Fe}_3\text{O}_4@ \text{SiO}_2$ -PSI nanoparticles showed relatively homogenous dispersion into the polyimide matrix. However, some aggregation was observed due to the interaction between the magnetic nanoparticles.

3.6 Component Analysis of PIEN 10b

PIEN 10b nanoparticles were chosen as a representative and assayed by EDS analysis (Fig. 7). Si, O, C, N

and Fe signals were clearly observed in the EDS analysis of this nanocomposite. The peak related to Si is a little stronger than Fe peak proving that Fe_3O_4 nanoparticles were trapped by SiO_2 shell. The EDS analysis confirmed that this nanocomposite was successfully synthesized.

As can be seen in the EDS mapping of this nanocomposite (Fig. 8), the nanoparticles were dispersed uniformly and no aggregation happened between them.



Fig. 6 TEM image of PIEN 10b nanocomposite

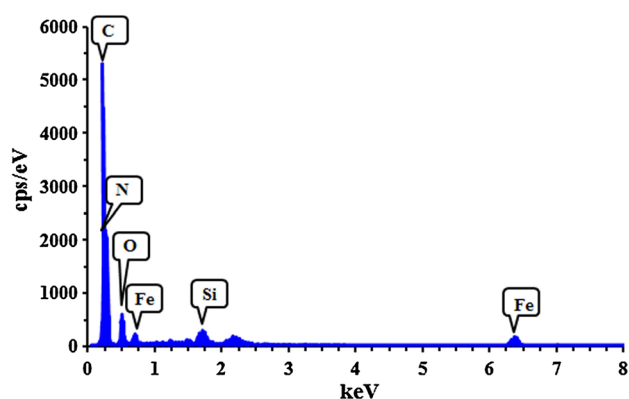


Fig. 7 The EDS spectrum of PIEN 10b nanocomposite

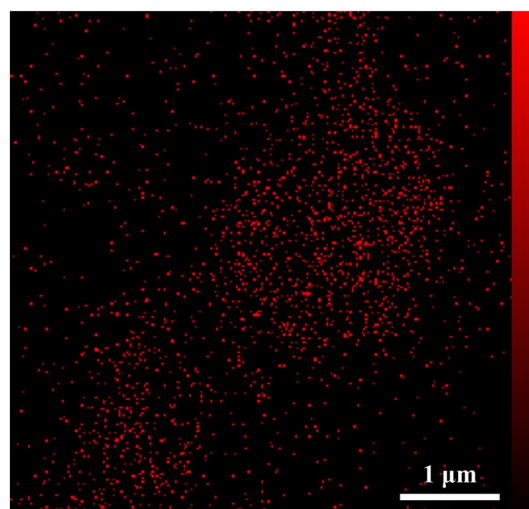


Fig. 8 EDS mapping of PIEN 10b nanocomposite

3.7 XRD Measurements

Figure 9 shows the XRD measurements of Fe_3O_4 (Fig. 9a), $\text{Fe}_3\text{O}_4@\text{SiO}_2\text{-PSI}$ (Fig. 9b), PIEN 10a (Fig. 9c) and PIEN 10b (Fig. 9d). The same patterns were observed for all four compounds, confirming that the crystalline spinel ferrite core remained intact during the modifications. According to the XRD data of the synthesized magnetic nanoparticles, the characteristic peaks were observed at $2\theta = 30.4, 35.7, 43.3, 53.9, 57.3, 63.0,$ and 74.5 which were assigned to the (220), (311), (400), (422), (511), (440) and (533) planes of Fe_3O_4 nanoparticles, respectively. Also, the XRD data matched well with the standard Fe_3O_4 sample (JCPDS card No.85-1436). All of this information confirmed that the nanoparticles were pure and had cubic spinel structures. The broad peak observed at $2\theta = 20\text{--}27$ were related to the amorphous silica phase structure in the shell of the silica-coated Fe_3O_4 nanoparticles. This peak existed in the XRD measurements of all of the compounds except for Fe_3O_4 , indicating the successful grafting of SiO_2 on the surface of the magnetic

nanoparticles. The crystallite size of magnetic nanoparticles can be determined by Scherrer's equation ($D = 0.9\lambda/\beta\cos\theta$), where D is the average crystalline size, λ represents the X-ray wave-length (0.154 nm), β denotes the full width in radian subtended by the half maximum intensity width of the powder peak for instance (311), and θ is related to the Bragg's angle of the (311) peak in degree [29]. According to this equation, the average size of the magnetic nanocomposites was calculated to be equal to 13.8 nm which agreed well with the average particle size obtained by TEM measurements (Fig. 6). The amorphous phase of polymers usually causes a broad peak at $2\theta = 15\text{--}28$. This peak could overlap with the peak related to the amorphous silica phase. Also, the intensity of characteristic reflections related to Fe_3O_4 in the PIEN 10b were lower than those of PIEN 10a due to more chemical interactions between the polymer chains and functionalized $\text{Fe}_3\text{O}_4@\text{SiO}_2\text{-PSI}$ [30].

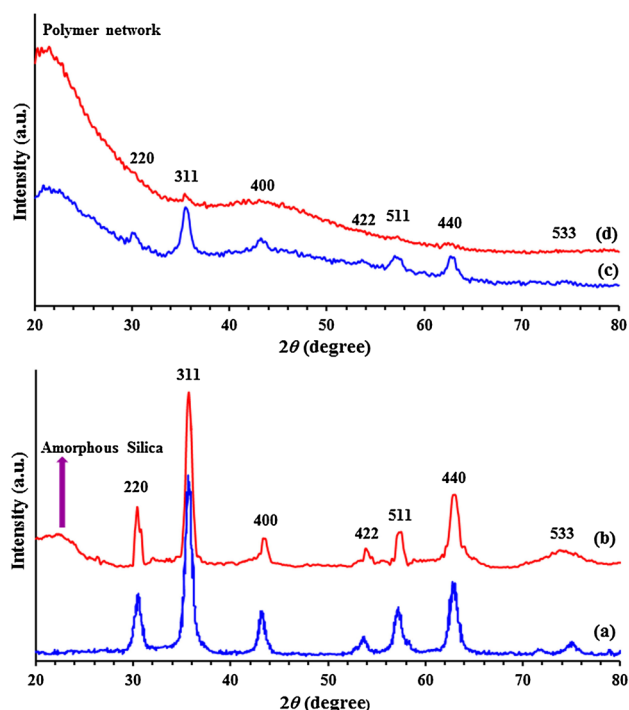


Fig. 9 The XRD pattern of Fe_3O_4 (a), $\text{Fe}_3\text{O}_4@SiO_2$ -PSI (b), PIEN 10a (c) and PIEN 10b (d)

3.8 Vibrating Sample Magnetometer (VSM) Studies

Figure 10 depicts M–H curves (hysteresis loops) of PIEN 10a (Fig. 10a) and PIEN 10b (Fig. 10b). In general, hysteresis curves can be used for obtaining important information about the magnetic properties of materials; including the saturation magnetization (M_s), remanent magnetization (M_r) and coercivity (H_c). The magnetization of the samples reached to saturation at high fields of up to ± 8000 Oe. In addition, saturation magnetization (M_s) of both PIEN 10a and PIEN 10b reduced from 1.63 to 0.32 emu g^{-1} because the nanoparticles were coated by silica shell and functionalized with the polymer (XBPEI). The magnetic properties of ferromagnetic particles strongly depend on their sizes. Ferromagnetic particles with diameter below 128 nm (especially, those with size of less than 30 nm) possess superparamagnetic properties [31]. Superparamagnetic nanoparticles tend to have a very large magnetic susceptibility while their H_c and M_r parameters are very low. M_r and H_c for PIEN 10a and PIEN 10b nanoparticles are close to zero ($M_r = 0.02$ and 0.005 emu g^{-1} , $H_c = 3$ and 6 Oe, respectively) so both PIEN 10a and PIEN 10b possess superparamagnetic properties. The results of VSM analysis were in good agreement with those of XRD and TEM analyses.

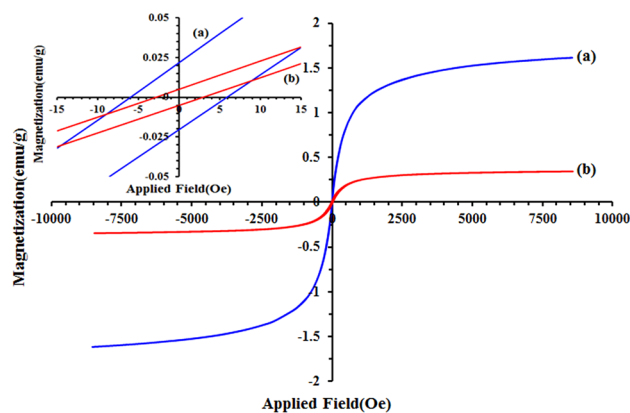


Fig. 10 Magnetization curves for the prepared PIEN 10a (a) and PIEN 10b (b)

3.9 Thermogravimetric Analyses (TGA)

The thermal properties of the prepared XBPEI and PIENs were studied by using TGA under the nitrogen atmosphere (Fig. 11; Table 1). The thermal stability of these compounds investigated in the range of 150 – 850 °C at a heating rate of 10 °C min^{-1} . The decomposition patterns of XBPEI and PIENs were the same. Typically, two important weight-loss steps took place in the TGA curves of all of the samples. The first step, which showed a low amount of mass loss below 275 °C, was related to the removal of physically adsorbed solvent and surface hydroxyl groups. The second step, which included a significant weight loss in the range 275 – 800 °C, was due to the degradation of the main XBPEI structure.

The TGA data; including temperatures at which 5% (T_5) and 10% (T_{10}) degradation occurred and also the char yields at 800 °C; were summarized in Table 1. As can be seen in this table, the char yields of XBPEI, PIEN 10a and PIEN 10b were about 34.6, 39.3 and 47%, respectively. These data proved that the presence of xanthene ring, ether and methyl groups in the backbone of the compounds made them have good thermal stability and good char yields. Furthermore,

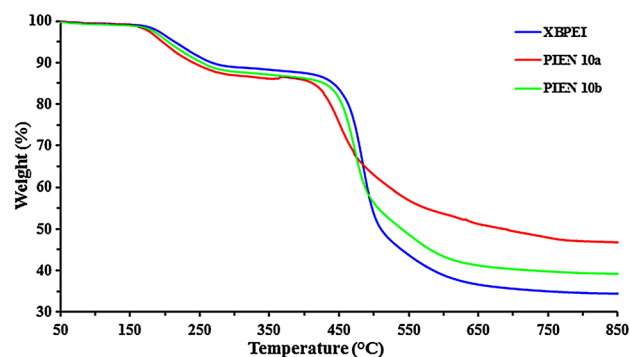


Fig. 11 TGA curves of the polymer and nanocomposites

Table 1 Thermal characteristic data of the polymer and magnetic nanocomposites

Samples	T ₅ ^a	T ₁₀ ^a	Char yield ^b	LOI ^c
XBPEI	204	253	34.6	31.3
PIEN 10a	189	229	39.3	33.2
PIEN 10b	196	241	47	36.3

^aTemperature at which 5 or 10% weight loss was recorded by TGA at heating rate of 10 °C min⁻¹ under N₂

^bWeight percentage of material left after TGA analysis at a maximum temperature of 700 °C

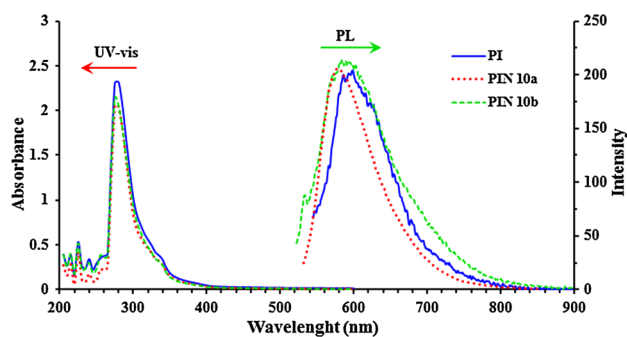
^cCalculated by equation of Van Krevelen and Hoftzyer

the introduction of inorganic components into the polymer matrix increased the char yields and consequently, the thermal stability of the polymer. According to the data summarized in Table 1, not only PIEN 10b had a higher char yield than PIEN 10a but also T₅ and T₁₀ parameters of PIEN 10b were higher than those of PIEN 10a. These data proved that PIEN 10b was thermally more stable than PIEN 10a. In fact, the higher stability of PIEN 10b could be due to better dispersion of Fe₃O₄@SiO₂-PSI nanoparticles in the polymer matrix and also better interaction of these nanoparticles with the polymer matrix. Moreover, the high compatibility and hydrogen bonds of Fe₃O₄@SiO₂-PSI and XBPEI caused a physical barrier effect. This effect slowed down the diffusion of pyrolysis products [26, 31]. Consequently, PIEN 10b exhibited superior thermal properties.

Generally, materials with limited oxygen index (LOI) higher than 26 show self-extinguishing behavior and are considered flame retardant. According to Van Krevelen and Hoftzyer equation (LOI = 17.5 + 0.4CR; where CR is Char yield), LOI values can be calculated by using the amount of char yields [32]. Based on this formula, LOI values of XBPEI, PIEN 10a and PIEN 10b were obtained to be 31.3, 33.2 and 36.3%, respectively so these compounds were recognized as self-extinguishing materials.

3.10 Optical Properties of XBPEI and the Magnetic Nanocomposites

UV-Vis and photoluminescence spectroscopies were used to investigate the optical properties of XBPEI, PIEN 10a and PIEN 10b. Figure 12 shows the UV-Vis and photoluminescence spectra of these compounds in the solution phase (in DMF). The UV-Vis spectra of the poly(ether-imide) showed a strong absorption band at 280 nm which were due to π - π^* transition resulting from the conjugation between the nitrogen and oxygen atoms and the aromatic rings [31]. The same absorption bands were also observed in the UV-Vis spectra of PIEN 10a and PIEN 10b (at 275 nm) confirming that all of these compounds possess the same optical properties.

**Fig. 12** UV-Vis and PL spectra of the neat polymer and nanocomposites

As can be seen in Fig. 12, the intensity of these absorption bands in the spectra of PIENs was lower than that of the neat polymer. This difference can be due to the trapped electron density resulting from high interaction between nanoparticles and the polymer chain.

Photoluminescence spectrum of the neat polymer showed a strong fluorescence at around 600 nm when the polymer was excited at 280 nm. This emission was due to the presence of xanthene groups in the structure of these compounds. The nanocomposites showed the same fluorescence properties and the position of the peaks almost didn't change upon loading the nanoparticles in the polyimide matrix.

4 Conclusion

In conclusion, heat resistant and superparamagnetic poly(ether-imide)/Fe₃O₄ (PIEN 10a) and poly(ether-imide)/Fe₃O₄@SiO₂-PSI (PIEN 10b) nanocomposites were successfully synthesized. Also, the thermal stability of these nanocomposites was investigated by using TGA and compared to those of the neat poly(ether-imide). TGA results revealed that incorporation of Fe₃O₄ and Fe₃O₄@SiO₂-PSI in the polymer matrix improved its thermal properties. Fe₃O₄@SiO₂-PSI showed even better effect than the unmodified Fe₃O₄ on the thermal stability of the nanocomposites. The higher interactions between Fe₃O₄@SiO₂-PSI nanoparticles and the polymer chains can be the main reason for this fact. Thus these nanocomposites were classified as new processable high performance materials. Besides, the magnetic properties of these nanocomposites were studied by using VSM and alternating gradient force magnetometer confirmed that both of these nanocomposites showed superparamagnetic behavior.

Acknowledgements We gratefully acknowledge financial support from the Research Council of Arak University.

Compliance with Ethical Standards

Conflict of interest The authors declare that they have no conflict of interest.

References

1. X. Wan, Y. Zhan, Z. Long, G. Zeng, Y. Ren, Y. He, Appl. Surf. Sci. **425**, 905 (2017)
2. H. Moghanian, A. Mobinikhaledi, Z. Baharangiz, J. Polym. Res. **21**, 513 (2014)
3. H. Kavas, M. Gunay, A. Baykal, M.S. Toprak, H. Sozeri, B. Aktas, J. Inorg. Organomet. Polym. Mater. **23**, 306 (2013)
4. H.M.Z.H. El Ghandoor, M.M.H. Khalil, M.I.M. Ismail, Int. J. Electrochem. Sci. **7**, 5734 (2012)
5. A. Ito, Y. Kuga, H. Honda, H. Kikkawa, A. Horiuchi, Y. Watanabe, T. Kobayashi, Cancer Lett. **212**, 167 (2004)
6. S. Komarneni, W. Hu, Y.D. Noh, A. Van Orden, S. Feng, C. Wei, H. Pang, F. Gao, Q. Lu, H. Katsuki, Ceram. Int. **38**, 2563 (2012)
7. S.K. Ramasahayam, G. Gunawan, C. Finlay, T. Viswanathan, Water Air Soil Pollut. **223**, 4853 (2012)
8. Y. Zhou, S. Wang, B. Ding, Z. Yang, Chem. Eng. J. **138**, 578 (2008)
9. D. Ding, X. Yan, X. Zhang, Q. He, B. Qiu, D. Jiang, H. Wei, J. Guo, A. Umar, L. Sun, Q. Wang, M.A. Khan, D.P. Young, X. Zhang, B. Weeks, T.C. Ho, Z. Guo, S. Wei, Superlattices Microstruct. **85**, 305 (2015)
10. G.R. Ferreira, T. Segura, F.G.S. Júnior, A.P. Umpierre, F. Machado, Eur. Polym. J. **48**(12), 2050 (2012)
11. J.S. Neves, J.F.G. de Souza, P.A.Z. Suarez, A.P. Umpierre, F. Machado, Macromol. Mater. Eng. **296**(12), 1107 (2011)
12. M. Ashjari, A.R. Mahdavian, N. Golshan Ebrahimi, Y. Mosleh, J. Inorg. Organomet. Polym. Mater. **20**, 213 (2010)
13. Y. Yang, X. Jiang, J. Chao, C. Song, B. Liu, D. Zhu, Y. Sun, B. Yang, Q. Zhang, Y. Chen, L. Wang, Sci. China Mater. (2017). doi:10.1007/s40843-017-9022-1
14. X. Peng, W. Zhang, L. Gai, H. Jiang, Y. Tian, Russ. J. Phys. Chem. A **90**(8), 1656 (2016)
15. Y. Lu, Y. Yin, B.T. Mayers, Y. Xia, Nano Lett. **2**, 183 (2002)
16. L. Yi, C. Li, W. Huang, D. Yan, Polymer **80**, 67 (2015)
17. D. Wilson, H.D. Stenzenberger, P.M. Hergenrother, *Polyimides* (Chapman and Hall, New York, 1990), p. 58
18. M.K. Ghosh, K.L. Mittal, *Polyimides Fundamentals and Applications* (Marcel Decker, New York, 1996), p. 7
19. A.M. Díez-Pascual, M. Naffakh, C. Marco, G. Ellis, M.A. Gómez-Fatou, Prog. Mater. Sci. **57**, 1106 (2012)
20. T.J. Fai, J.E. Mark, P.N. Prasad, *Polymers and Other Advanced Materials Emerging Technologies and Business Opportunities*. (Springer, New York, 1996)
21. K. Faghihi, H. Moghanian, Polym. Bull. **65**(4), 319 (2010)
22. H.L. Tyan, K.H. Wei, T.E. Hsieh, J. Polym. Sci. B **38**, 2873 (2000)
23. C.M. Leu, Y.T. Chang, K.H. Wei, Macromolecules **36**, 9122 (2003)
24. M.A. Saeed, Z. Akhter, M. Saif Ullah Khan, N. Iqbal, M.S. Butt, Polym. Degrad. Stab **93**, 1762 (2008)
25. X. Zhao, Y.F. Li, S.J. Zhang, Y. Shao, X.L. Wang, Polymer **48**, 5241 (2007)
26. M. Shabaniyan, H. Moghanian, M. Khaleghi, M. Hajibeygi, H.A. Khonakdar, H. Vahabi, RSC Adv. **6**, 112568 (2016)
27. K. Can, M. Ozmen, M. Ersoz, Colloids Surf. B **71**, 154 (2009)
28. W. StÖşber, A. Fink, E.J. Bohn, J. Colloid Interface Sci. **26**, 62 (1968)
29. G. Feng, D. Hu, L. Yang, Y. Cui, X. Cui, H. Li, Sep. Purif. Technol. **74**, 253 (2010)
30. M. Shabaniyan, Z. Mirzakhaniyan, H. Moghanian, M. Hajibeygi, H. Salimi, H.A. Khonakdar, J. Therm. Anal. Calorim. **129**(1), 147 (2017)
31. A.H. Lu, E.L. Salabas, F. Schüth, Angew. Chem. Int. Ed. **46**, 1222 (2007)
32. D.W. Van Krevelen, P.J. Hoftyzer, *Properties of Polymers, Their Estimation and Correlation with Chemical Structure*, 3th edn. (Elsevier Scientific Publishing, New York, 1976)